ARTICLE

ACS chemical biology

An Oxazole-Based Small-Molecule Stat3 Inhibitor Modulates Stat3 Stability and Processing and Induces Antitumor Cell Effects

Khandaker A. Z. Siddiquee[†,‡], Patrick T. Gunning[§], Matthew Glenn[§], William P. Katt[§], Shumin Zhang[¶], Christopher Schroeck[¶], Said M. Sebti[∥,⊥⊥,††], Richard Jove[‡‡,§§], Andrew D. Hamilton[§], and James Turkson[†,‡,*]

[†]BioMolecular Science Center and, [‡]Department of Molecular Biology and Microbiology, University of Central Florida College of Medicine, Orlando, Florida 32826, [§]Department of Chemistry, Yale University, New Haven, Connecticut 06520, [¶]Molecular Oncology and, [∥]Drug Discovery Programs, H. Lee Moffitt Cancer Center and Research Institute and Departments of, [⊥⊥]Interdisciplinary Oncology, [††]Biochemistry and Molecular Biology, University of South Florida College of Medicine, Tampa, Florida 33612, [‡‡]Developmental Cancer Therapeutics Program, City of Hope Comprehensive Cancer Center, City of Hope, Duarte, California 91010, and [§§]Division of Molecular Medicine, Beckman Research Institute, City of Hope, Duarte, California 91010

ABSTRACT Stat3 is hyperactivated in many human tumors and represents a valid target for anticancer drug design. We present a novel small-molecule Stat3 inhibitor, S3I-M2001, and describe the dynamics of intracellular processing of activated Stat3 within the context of the biochemical and biological effects of the Stat3 inhibitor. S3I-M2001 is an oxazole-based peptidomimetic of the Stat3 Src homology (SH) 2 domain-binding phosphotyrosine peptide that selectively disrupts active Stat3:Stat3 dimers. Consequently, hyperactivated Stat3, which hitherto occurs as "dotlike" structures of nuclear bodies, undergoes an early aggregation into nonfunctional perinuclear aggresomes and a late-phase proteasome-mediated degradation in malignant cells treated with S3I-M2001. Thus, S3I-M2001 inhibited Stat3-dependent transcriptional regulation of tumor survival genes, such as Bcl-xL. Furthermore, Stat3-dependent malignant transformation, survival, and migration and invasion of mouse and human cancer cells harboring persistently activated Stat3 were inhibited by S3I-M2001. Finally, S3I-M2001 inhibited growth of human breast tumor xenografts. The study identifies a novel Stat3 inhibitor, S3I-M2001, with antitumor cell effects mediated in part through a biphasic loss of functional Stat3. The study represents the first on intracellular Stat3 stability and processing following inhibition by a small molecule that has significant antitumor activity.

The signal transducer and activator of transcription (STAT) family of proteins was originally discovered as latent cytoplasmic transcription factors that mediate cytokine and growth factor responses (*1, 2*). Seven members of the family, Stat1, Stat2, Stat3, Stat4, Stat5a and Stat5b, and Stat6, mediate several physiological effects including growth and differentiation, survival, development, and inflammation. STATs are SH2 domain-containing proteins. Upon ligand-binding to cytokine or growth factor receptors, STATs become phosphorylated on critical Tyr residue (Tyr705 for Stat3) by growth factor receptors, cytoplasmic Janus kinases (Jaks), or Src family kinases. Two phosphorylated and activated STAT monomers dimerize through reciprocal pTyr-SH2 domain interactions, translocate to the nucleus, and bind to specific DNA-response elements of target genes, thereby inducing gene transcription (*1, 2*). In contrast to normal STAT signaling, many human solid and hematological tumors harbor aberrant Stat3 activity (see refs (*3–8*) for reviews). Constitutive Stat3 activity mediates dysregulated growth and survival, angiogenesis, as well as suppresses the host's immune surveillance of the tumor, making constitutively active Stat3 a critical molecular mediator of carcinogenesis and tumor progression.

Genetic and other molecular evidence reveals persistent Tyr phosphorylation of Stat3 is mediated by aberrant upstream Tyr kinases and shows cancer cell requirement for constitutively active and dimerized Stat3 for tumor maintenance and progression. Thus, in numer-

*Corresponding author, jturkson@mail.ucf.edu.

Received for review June 7, 2007.
Published online December 21, 2007
10.1021/cb7001973 CCC: $37.00

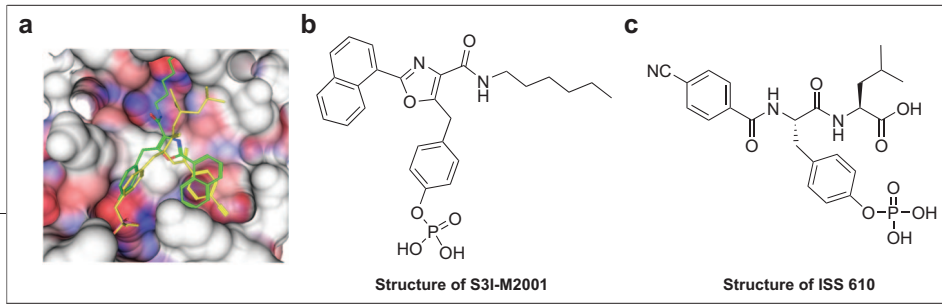

Figure 1. Computational modeling of S3I-M2001 bound to the Stat3 SH2 domain and S3I-M2001 chemical structure: a) S3I-M2001 (green) docked to the SH2 domain of Stat3, along with Stat3 peptidomimetic inhibitor, ISS 610 (yellow) (*10*), and chemical structure of b) S3I-M2001 or c) ISS 610.

ous proof-of-concept studies (*9*–*13*), inhibition of Stat3 activation or disruption of dimerization induces cancer cell death and tumor regression. How aberrant Stat3 is regulated for meeting the tumor-specific requirements in malignant cells remains undefined. There have been no studies into defining the molecular details of how malignant cells regulate aberrant Stat3 and how this regulation changes upon Stat3 inhibition prior to the onset of phenotypic changes, although knowing these events will facilitate efforts in modulating aberrant Stat3 for managing human cancers. Small-molecule Stat3 inhibitors thus provide tools for probing the molecular dynamics of the cellular processing of Stat3 to understand Stat3′s role as a signaling intermediate and a molecular mediator of the events leading to carcinogenesis and malignant progression.

The computational analysis of the interaction between the Stat3 SH2 domain-binding pTyr peptide sequence and the SH2 domain, per the X-ray crystal structure of Stat3β bound to DNA (*14*), can generate valuable information about key structural requirements for the Stat3:Stat3 dimer formation that will facilitate the design of effective small molecules to disrupt the dimer. Such molecules can be used for therapeutic purposes and as tools for investigating the regulation of Stat3 protein. In the molecular modeling of the Stat3 pTyr-SH2 domain interaction, the peptidomimetic inhibitor, ISS 610 (*10*) derived from the Stat3 SH2 domain-binding pTyr (Y*) peptide, PY*LKTK (*9*), was used as a chemical probe for interrogating the Stat3:Stat3 dimer interface in order to derive nonpeptide mimics. We describe the design and characterization of an oxazole-based peptidomimetic, S3I-M2001, as a selective disruptor of Stat3:Stat3 dimerization and inhibitor of Stat3 activation and, the study of the stability and intracellular processing of aberrant Stat3 within the context of the activity of S3I-M2001 as a Stat3 inhibitor.

RESULTS AND DISCUSSION

Computational Modeling of the Stat3 SH2 Domain-ISS 610 Complex. Close structural analysis of the lowest genetic optimization for ligand docking (GOLD) (*15*) conformation of ISS 610 (yellow) (IC_{50} = 42 μM for inhibition of Stat3:Stat3) (*10*) bound within the Stat3 SH2 domain (Figure 1, panel a), per the X-ray crystal structure of Stat3β (*14*), indicated key structural requirements for hydrophobic, hydrogen-bonding, and electrostatic interactions critical for tight binding. Appropriate candidate binders are suitably substituted heterocyclic systems that reproduce the critical ISS 610-Stat3 interactions. Hence, S3I-M2001 (Figure 1, panel b), which contained a central oxazole core with two hydrophobic substituents to complement the relatively hydrophobic protein surface and a pTyr group to bind to the phosphate recognition residues of the third pocket, and which superimposes well with the parent ISS 610 docked into the same SH2 cavity (Figure 1, panel a). Docking studies of S3I-M2001 identified significant complementary interactions between the protein surface and the molecule. The pTyr moiety is bound tightly within a hydrophilic cleft composed of Arg609, Ser613, and Ser611. This important contact may predetermine the subsequent orientations of the two lipophilic groups within the hydrophobic regions of the SH2 domain. The naphthyl appendage makes significant contact with the Ile634 side chain, and the lipophilic hexyl substituent is partially encased within a hydrophobic channel composed primarily of Phe716 and Trp623. Positive cooperativity may exist between these subunits to provide a highly potent binding agent for the SH2 active site. (See Supporting Information, Results and Discussion for more on this subject.)

Stat3-Inhibitory Property of S3I-M2001. Per DNA-binding assay/electrophoretic mobility shift assay (EMSA) analysis (see Methods for details), S3I-M2001 favorably disrupts Stat3 activity *in vitro* in nuclear extracts containing activated Stat3 (Figure 2, panel a, left) or in lysates from Sf-9 cells containing activated Stat3 (Supplementary Figure S1), and preferentially inhibits Stat3 activity over Stat1 by 2-fold (IC_{50} values (μM), Stat3:Stat3, 79 ± 09; Stat1:Stat3, 92 ± 11; and Stat1:Stat1, 159 ± 06) (Figure 2, panel a, middle and right). Similarly, per DNA-binding assay/EMSA analysis (Figure 2, panel b), SDS-PAGE/Western blot (Figure 2, panel c) and immunocytostaining (Supplementary Figure S2) analyses, S3I-M2001 inhibited constitutive Stat3 Tyr phosphorylation and activation in the NIH3T3/v-Src and the human breast cancer MDA-MB-231 and MDA-MB-435 cell lines that harbor constitutively active Stat3 (*16*–*18*) (Figure 2, panel b, lanes 1–13, and

Figure 2, panel c, lanes 1–6), and preferentially inhibited the epidermal growth factor (rhEGF)-induced Stat3 activation over that of Stat1 in the mouse fibroblasts overexpressing the human EGF receptor (NIH3T3/hEGFR) (Figure 2, panel b, right). Supershift analysis with anti-Stat3 antibody shows protein:DNA probe complex contains Stat3 (Figure 2, panel b, lane 8). By contrast, the pJak1, pSrc, and pErk1/2 (MAPKs) in NIH3T3/v-Src fibroblasts are not repressed by S3I-M2001 (Figure 2, panel c, lanes 7–12), indicating minimal effect on non-Stat3-related proteins. Furthermore, transient transfection and luciferase reporter studies showed S3I-M2001 inhibited v-Src-induced Stat3-dependent pLucTKS3 luciferase reporter, but not the v-Src-induced Stat3-independent pLucSRE luciferase reporter (*17, 19*), in a similar manner to the effect of the transient coexpression of the dominant-negative Stat3β (Figure 3, panel a) (*17, 19*).

To confirm the disruption of Stat3:Stat3 dimerization, the previously reported dissociation–reassociation analysis (*9, 10, 20*) was performed using pooled cell lysates of independently prepared lysates of activated Stat1 and Stat3 (details are provided in Supporting Information). Stat1 or Stat3 DNA-binding activity was evident in their respective cell lysates (Figure 3, panel b, lanes 1 and 2) and present together in the pooled lysates (Figure 3, panel b, lane 3). Pooled lysate treated with S3I-M2001 showed a concentration-dependent diminution of Stat3:Stat3 DNA-binding activity (Figure 3, panel b, lanes 3–6) ahead of a diminishing Stat1:Stat1 homodimer activity (Figure 3, panel b, lanes 5–7), and the appearance of an intermediate band corresponding to Stat1:Stat3 heterodimer activity, which was hitherto not present (Figure 3, panel b, lanes 5 and 6). The formation of the Stat1:Stat3 band is due to the reassociation between transient monomers of active Stat3 and Stat1 (*9, 10*). The disappearance of the activities for Stat3:Stat3 (Figure 3, panel b, lanes 5–7) and Stat1:Stat3 (Figure 3, panel b, lane 7) is due to dimer disruption, as previously observed for ISS 610 (*9, 10*), and suggests a preferential disruption of Stat3:Stat3 over Stat1:Stat1 homodimer (Figure 2, panel a, middle and right). By contrast, *in vitro* enzyme-linked immunosorbent assay (ELISA) study of the pTyr-SH2 domain interaction between the unrelated Lck SH2-GST and its cognate phosphopeptide, biotinyl-ϵ-Ac-EPQpYEEIEL-OH (*21*) (Figure 3, panel c, fourth bar) showed minimal effect of S3I-M2001 at 30 or 100 μM (Figure 3, panel c, compare bars 5 and 6 to bar 4). Thus, S3I-M2001 selectively disrupts Stat3:Stat3 dimers, thereby inhibiting Stat3 DNA-binding and transcriptional activities, while not affecting the Lck-SH2 domain function. On whether disruption of Stat3 dimerization inhibits nuclear translocation, immunofluorescence imaging/confocal microscopy for the nuclear localization of Stat3 in EGF-stimulated NIH3T3/hEGFR mouse fibroblasts revealed a strong EGF-induced nuclear staining of Stat3 in the absence of S3I-M2001 (Figure 3, panel d, third panel from left), which was significantly attenuated upon treatment of cells with S3I-M2001 (Figure 3, panel d, fourth from left), suggesting inhibition of Stat3 activation blocks its nuclear localization.

Intracellular Stat3 Processing. Malignant cell requirement for persistently active Stat3 for the maintenance of the malignant phenotype is well-established (*17–19, 22, 23*). How tumor cells regulate Stat3 to meet this requirement, however, is not defined. Moreover, while the inhibition of aberrant Stat3 activity results in malignant cells demise (*9–13*), the molecular details of Stat3 cellular processing and the fate of the protein within the context of such an inhibition have not been explored. Given S3I-M2001's specific anti-Stat3 properties, it was used to probe the intracellular processing and localization dynamics of aberrant Stat3. Fluorescent microscopy (Nikon Eclipse TE200) (Figure 4, panel a) and laser scanning confocal microscopy (Figure 4, panels b–e) of the NIH3T3/v-Src fibroblasts stably transfected with the yellow fluorescent protein (YFP)-tagged Stat3 (Stat3-YFP) plasmid (*24*) (NIH3T3/v-Src/Stat3-YFP) showed a stronger nuclear Stat3-YFP signal, consistent with constitutive Stat3 activation (Figure 4, panels a, b, and d, right, and e). Treatment with S3I-M2001 induced a time-dependent decrease in the Stat3-YFP fluorescence; there is no change in signal at 1 h treatment or less, while an increasing degree of Stat3 fluorescence loss becomes evident from 2 to 5 h, 100–300 μM S3I-M2001 treatment (Figure 4, panel a, time $t = 0$ to 6 h, left; arrows denote Stat3-YFP signal; Figure 4, panel b, second column from left compared to first, time $t = 0$ to 2 h; Figure 4, panel d, right, time $t = 0$ to 5 h)). Phase contrast microscopy showed cellular integrity was maintained (Figure 4, panel a, time $t = 0$ to 6 h, right; arrows identify cells remaining or originally positive for fluorescent signal). Protein degradation can result in fluorescence signal loss (*25*). Accordingly, the presence of MG132 proteasome inhibitor prevented the fluorescence loss (Figure 4, panel b, third column from left),

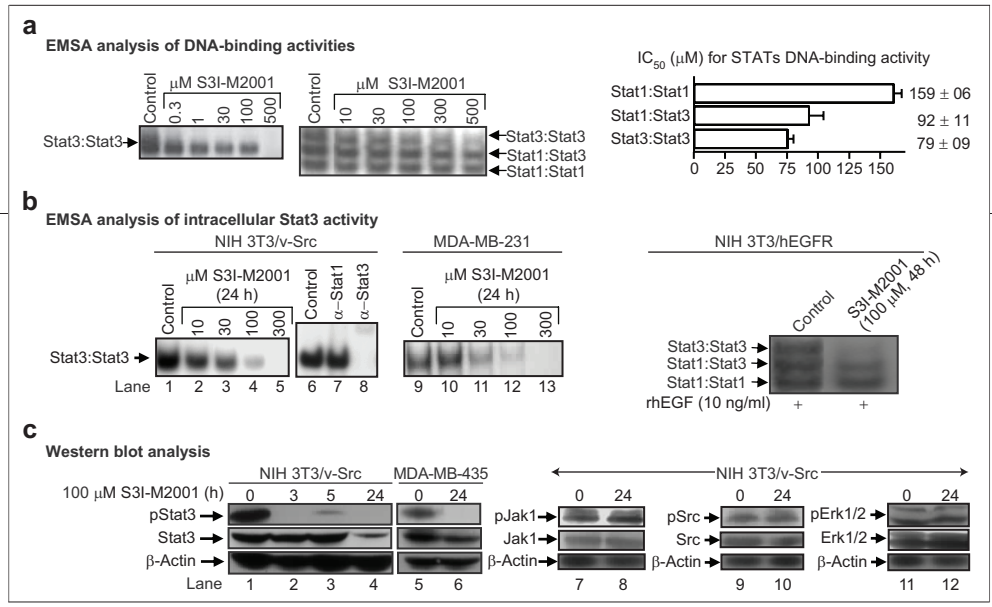

Figure 2. Effects of S3I-M2001 on STATs activation and on pJak1, pSrc, pErk1/2. a) EMSA analysis of STATs DNA-binding activities in nuclear extracts containing activated Stat3 (left panel) or Stat1 and Stat3 (middle panel) and pretreated with S3I-M2001 concentrations for 30 min at RT prior to incubation with radiolabeled hSIE oligonucleotide probe, and IC_{50} values for the inhibition of STATs DNA-binding activity *in vitro* (right panel) derived, as described in Methods. b) EMSA analysis of Stat3 DNA-binding activity in nuclear extracts from NIH3T3/v-Src or MDA-MB-231 cells, or from recombinant human EGF (rhEGF)-stimulated NIH3T3/hEGFR mouse fibroblasts treated with or without S3I-M2001. c) SDS-PAGE/Western blot analysis of whole-cell lysates prepared from S3I-M2001-treated or untreated NIH3T3/v-Src or MDA-MB-435 cells probing for pTyr705Stat3, Stat3, pJak1, Jak1, pSrc, Src, pErk1/2, Erk1/2, and β-Actin. Positions of STAT:DNA complex in gel, pTyrStat3 and Stat3 are labeled. Values are the mean and standard deviation of three replicate experiments. Data are representative of three independent studies. IC_{50} values were determined by quantifying by ImageQuant the bands corresponding to the STAT:DNA complexes; control lanes represent nuclear extracts untreated with S3I-M2001 or nuclear extract preparations from cells untreated with the compound.

while MG132 alone has no appreciable effect (Figure 4, panel b, fourth column from left), suggesting the Stat3 fluorescence decay may involve the ubiquitin-proteasome degradation pathway. In contrast, similar studies with the v-Src transformed fibroblasts stably expressing the non-Stat3 related green fluorescent protein (GFP) (NIH3T3v-Src/GFP) showed no evidence of GFP signal change by S3I-M2001 or the proteasome inhibitor MG132 (Figure 4, panel c, and Figure 4, panel d, left), thus excluding the possibility of nonspecific fluorescence quenching or photobleaching. Moreover, immunoblotting of whole-cell lysates from NIH3T3/v-Src/Stat3-YFP fibroblasts showed reduced Stat3-YFP expression in S3I-M2001-treated cells in 3 and 5 h, which was similarly partially restored when cells were cotreated with MG132 (Figure 5, panel a, lanes 3 and 4 *vs* lanes 5 and 6). That only a partial corresponding decrease in total Stat3 protein occurred (Figure 5, panel a, lanes 3 and 4) suggests a weak proteasome activity against total Stat3 protein. However, immunoblotting for ubiquitin of Stat3 immunoprecipitates (i.p.) from NIH3T3/v-Src fibroblasts showed a strong and time-dependent increase in the level of Stat3 ubiquitination following the S3I-M2001 treatment, which occurred in parallel with partial and strong Stat3 protein reductions at 5 and 24 h, respectively (Figure 5, panel b). These findings together raise the possibility there is an impairment of proteasome function (*26, 27*) at the early hours (<5 h) of S3I-M2001 treatment and suggests additional mechanisms contribute to the Stat3 fluorescence signal decay.

Protein misfolding can lead to ubiquitin-proteasome degradation, and aggregation into aggresomes (*25, 28–30*). Aggresomes can lead to fluorescence signal loss (*25*) and impairment of proteasome function (*26, 27*). Using laser scanning confocal microscopy, we observed that the specific loss of Stat3−YFP signal in the NIH3T3/v-Src/Stat3-YFP that follows S3I-M2001 treatment (Figure 4, panel d, right column, and panel e, right column, time $t = 0$ to 5 h) is accompanied by aggregated bodies, possibly aggresomes of Stat3−YFP, within 5 h of S3I-M2001 treatment (Figure 4, panel e, right bottom; red arrow denotes bodies). By contrast, Cisplatin treatment produced no such effect (Figure 4, panel e, middle column). Confirming these data, immunofluorescence imaging/confocal microscopy of Stat3 in NIH3T3/v-Src fibroblasts revealed that in contrast to the strong nuclear fluorescence of activated Stat3 protein that occurred in "dotlike" structures resembling nuclear bodies (*24*) and the low cytoplasmic signal in the untreated cells (Figure 6, panel a, control), a strongly reduced Stat3 fluorescence signal occurred that coincided with the appearance of perinuclear aggregated bodies, possibly aggresomes in the S3I-M2001-treated cells within 3 h and later, with a stronger aggresome formation at 24 h treatment (Figure 6, panel a, S3I-M2001, time $t = 0.5$ to 24 h). Thus, S3I-M2001 promotes the disruption of activated Stat3 from "dotlike" nuclear bodies (*24*) into perinuclear aggresomes, which may explain the apparent low proteasome-mediated degradation in the early period of S3I-M2001 treatment. The Stat3 aggresome formation and signal loss are events specific to S3I-M2001, because they are not induced by Cisplatin (Figure 6, panel a, Cisplatin) and occur in the early hours (<5 h)

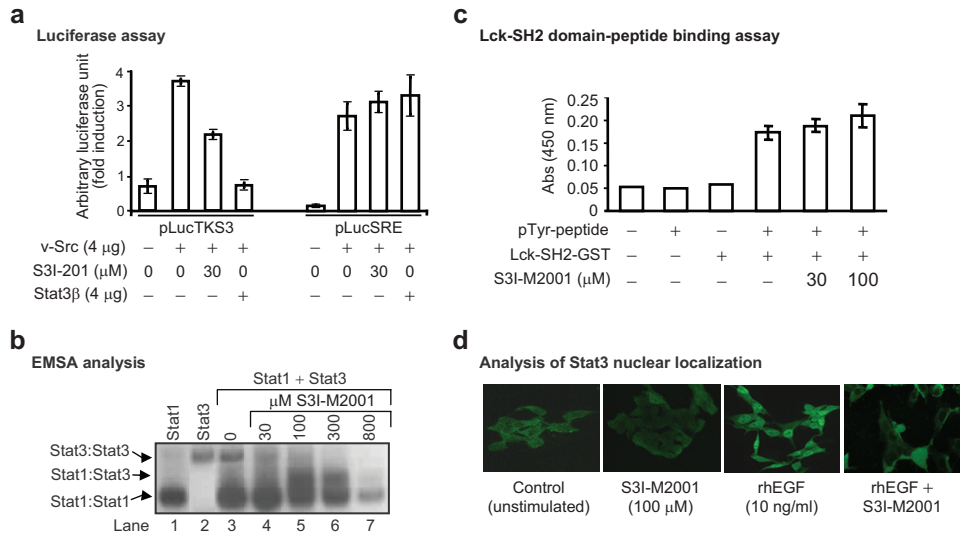

Figure 3. Effects of S3I-M2001 on Stat3 transcriptional activity and dimerization, and nuclear localization, and on the Lck-SH2 domain function. a) Luciferase reporter measurements in cytosolic extracts prepared from NIH3T3 fibroblasts transiently cotransfected with the Stat3-dependent (pLucTKS3) or the Stat3-independent (pLucSRE) luciferase reporter together with the v-Src plasmid with and without Stat3β plasmid and treated with or without S3I-M2001. b) EMSA analysis of STATs DNA-binding activities in independently prepared cell lysates of activated Stat1 or Stat3, or mixed pool of lysates of both proteins and pretreated with or without S3I-M2001 concentrations for 30 min at RT prior to incubation with radiolabeled hSIE oligonucleotide probe, as described in Methods. c) *In vitro* ELISA for the binding of Lck-SH2-GST to the conjugate biotinylated pTyr-peptide (EPQpYEEIEL) and effects of S3I-M2001. d) Immunofluorescence imaging/confocal microscopy of Stat3 nuclear localization in NIH3T3/hEGFR treated with or without 100 μM S3I-M2001 for 3 h prior to stimulation or unstimulation by EGF (rhEGF) for 10 min. Positions of STAT:DNA complex in gel are labeled. Values are the mean and standard deviation of six replicate experiments. Data are representative of three independent studies.

of treatment prior to change in cellular integrity (Figure 4, panel a, and data not shown). The resting of NIH3T3/v-Src fibroblasts for 2 h following a 5 h S3I-M2001 treatment led to a partial recovery of Stat3 signal, while aggresomes remained (Figure 6, panel b, top, compare right column *vs* middle column, 5 h treated cells without recovery *vs* control), suggesting the effect of S3I-M2001 still persisted in the 2 h following drug removal. By contrast, Stat3 immunofluorescence was completely recovered within 19 h of resting after 5 h of treatment (Figure 6, panel b, bottom, compare right column *vs* middle column, 5 h treated cells without recovery *vs* control), either because S3I-M2001's effect on Stat3 was reversible or that new Stat3 protein was synthesized. To investigate further and to demonstrate the perinuclear aggresome localization, immunofluorescence imaging/confocal microscopy was performed on NIH3T3/v-Src fibroblasts harboring constitutively active Stat3 to assess the colocalization with Hook2, an adaptor protein important for the association of cargos with dynein for the transport on microtubules and for aggresome formation (*28*). As expected, a strong nuclear Stat3 staining is observed (Figure 6, panel c, upper left), which contrasts a Hook2 expression that appears ubiquitous (Figure 6, panel c, upper middle), without any evidence of colocalization. By contrast, S3I-M2001 induced the formation of perinuclear aggregated bodies of Stat3 (Figure 6, panel c, bottom left), which colocalized with Hook2 (Figure 6, panel c, bottom middle and right; red arrows denote aggregated bodies), suggesting a possible association between the two proteins and implicating the Hook proteins in the Stat3 aggresome formation.

Together, our studies are the first on the localization dynamics and the molecular mechanisms for terminating Stat3 function in response to a small-molecule inhibitor. Two possible mechanisms may account for the loss of aberrant Stat3 function: one involves protein

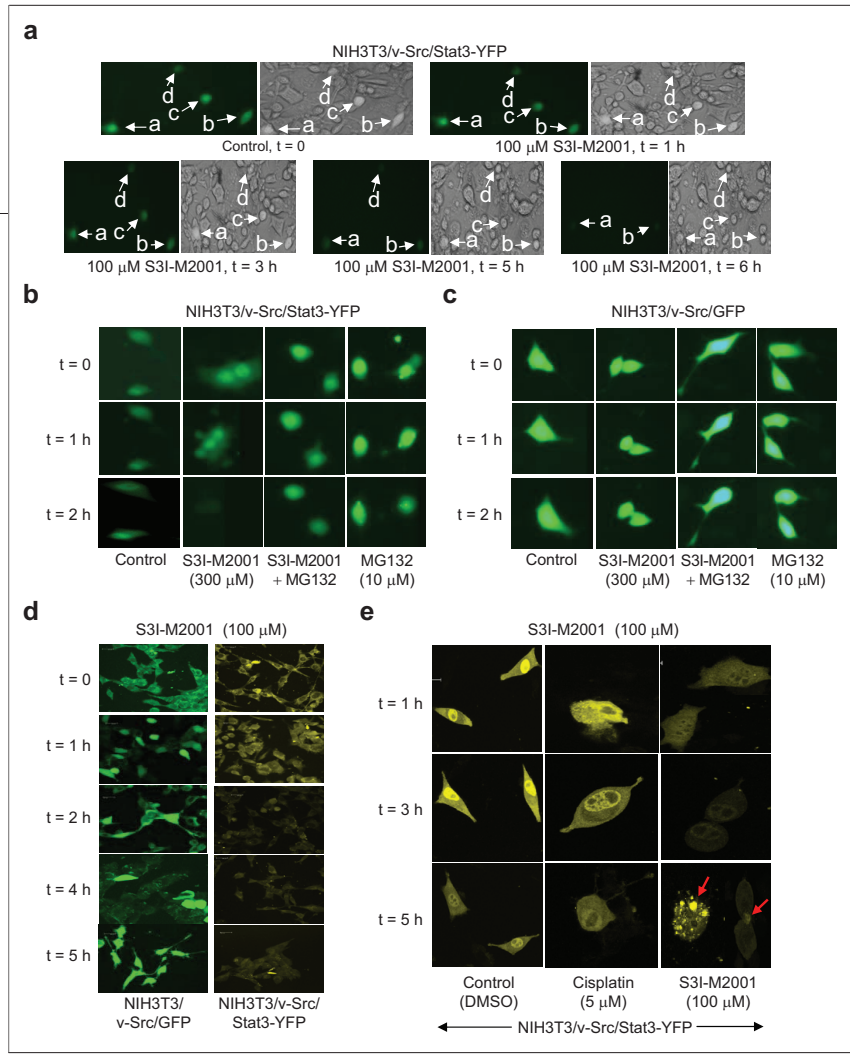

Figure 4. Fluorescence with confocal microscopy of intracellular Stat3 signal. Fluorescence microscopy of the NIH3T3/v-Src fibroblasts stably expressing the plasmids for a) and b) yellow fluorescent protein (YFP)-tagged Stat3 (NIH3T3/v-Src/Stat3-YFP) or c) green fluorescent protein (GFP) (NIH3T3/v-Src/GFP) and treated with or without S3I-M2001 for the indicated times in the presence or absence of the proteasome inhibitor, MG132 (1 h of pretreatment); and laser scanning confocal microscopy of d) NIH3T3/v-Src/GFP (left) or NIH3T3/v-Src/Stat3-YFP (right) or e) NIH3T3/v-Src/Stat3-YFP and treated with or without S3I-M2001 or Cisplatin for the indicated times. Fluorescence and confocal images were collected using Nikon Eclipse TE200 and Leica TCS SP5 microscopes, respectively. Arrows denote fluorescence or cells previously showing fluorescence, or aggregated Stat3-YFP. Data are representative of two to three independent studies.

events are irreversible and lead to a long-term loss of Stat3 function, with biological consequences. The perinuclear aggresome formation also suggests a nuclear-to-perinuclear exit of disrupted "activated" Stat3 by as yet undetermined mechanisms.

Suppression of Malignant Phenotype and Tumor Growth. Consistent with Stat3's importance in maintaining the malignant phenotype (*17*), WST-1 assay (Figure 7, panel a) and trypan blue exclusion/cell counting (data not shown) revealed S3I-M2001-induced growth inhibition and a greater than 2-fold selective loss of viability of the human breast (MDA-MB-435 and MDA-MB-231) and pancreatic (Panc-1) cancer cells, and the NIH3T3/v-Src fibroblasts, which all harbor constitutively active Stat3, with IC_{50} values in the range of 50–100 μM, compared to effects on normal NIH3T3 fibroblasts, and the human breast (MDA-MB-453) and pancreatic (MiaPaca-1) cancer cells that lack aberrant Stat3 (IC_{50} values of 120–300 μM) (Figure 7, panel a). Furthermore, S3I-M2001 blocked growth in soft-agar of the NIH3T3/v-Src and the pancreatic cancer, Panc-1 cells (Figure 7, panel b), and induced morphology changes in NIH3T3/v-Src (Supplementary Figure S3), in contrast to no appreciable effects on v-Ras transformed fibroblasts (NIH3T3/v-Ras) lacking constitutively active Stat3 (Figure 7, panel b). Terminal nucleotidyl transferase-mediated nick end labeling (TUNEL) (Figure 7, panel c) and Annexin V binding with flow cytometric analyses (Figure 7, panel d, first and third pairs of bars)

ubiquitination and an early aggregation into perinuclear aggresomes (*30*), and a late-phase proteasome-mediated degradation event, potentially a "quality control" mechanism for Stat3 (*31*), given its apparent unnatural state promoted by S3I-M2001. The effects of early aggresome formation may be reversible, while the late-phase

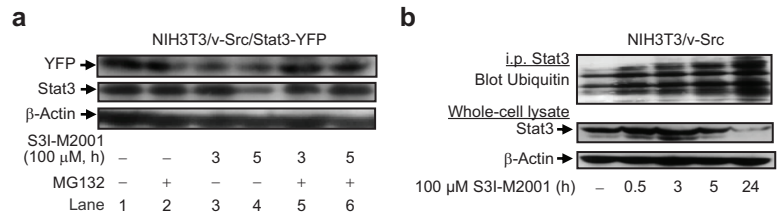

Figure 5. Immunoblotting analyses of intracellular Stat3 signal. SDS-PAGE/Western blot analysis a) of whole-cell lysates from NIH3T3/v-Src/Stat3-YFP probing for YFP, Stat3, or β-Actin and b) of Stat3 immunoprecipitates from NIH3T3/v-Src fibroblasts blotting for ubiquitin, or NIH3T3/v-Src whole-cell lysates blotting for Stat3 or β-Actin. Data are representative of two to three independent studies.

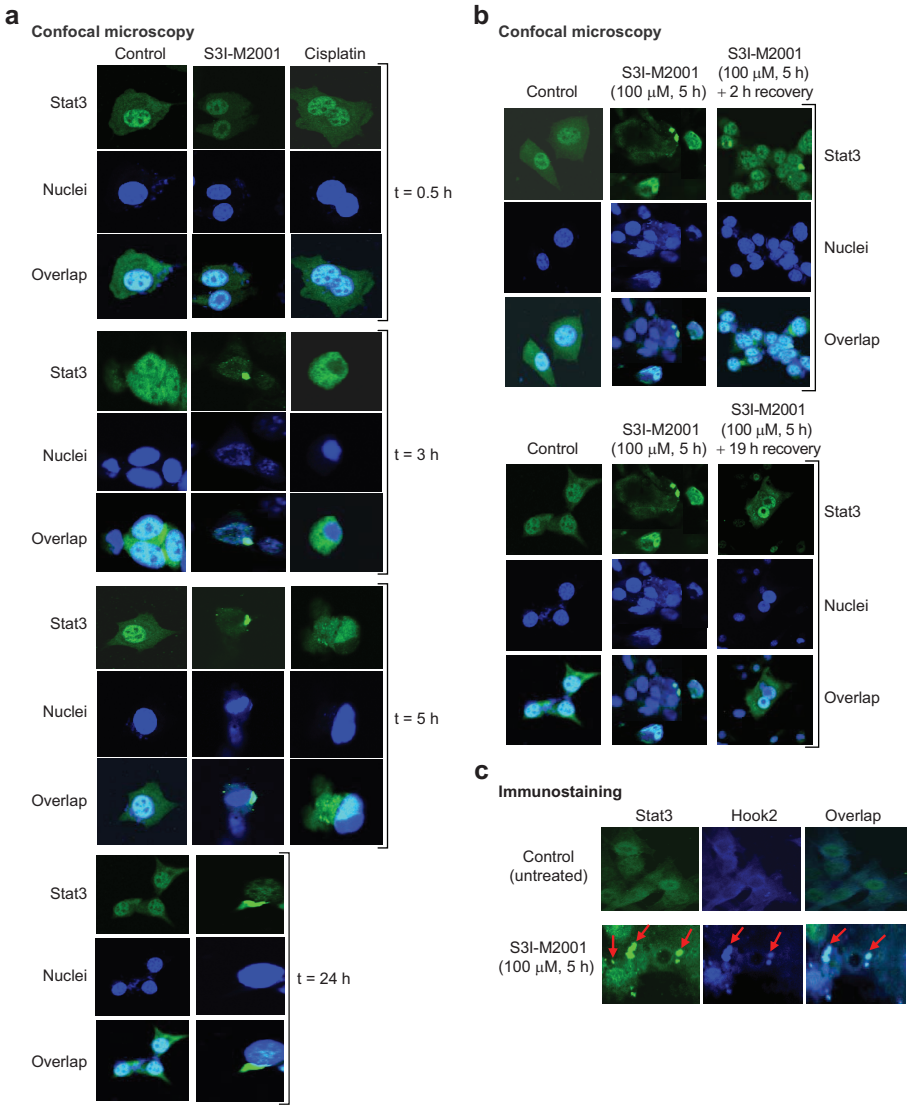

Figure 6. Immunofluorescence with laser scanning confocal imagining of Stat3 aggregation into perinuclear aggresomes induced by S3I-M2001. Immunofluorescence and confocal microscopy of NIH3T3/v-Src fibroblasts growing in culture treated with or without S3I-M2001 or Cisplatin for the indicated times: a) fixed and stained with rabbit anti-Stat3 antibody (green) or DAPI nuclear staining (blue); b) allowed to recover from the effects of S3I-M2001 for 2 or 19 h prior to fixing and staining for Stat3 or with DAPI; c) fixed and stained with rabbit antibody against Stat3 (green) or goat antibody against Hook2 (blue). Arrows denote aggregated Stat3 and localization of Hook2 protein. Images were captured using Leica TCS SP5 laser scanning confocal microscope and are representative of three independent experiments.

showed strong apoptosis in the NIH3T3/v-Src (3T3/v-Src) and MDA-MB-231 and MDA-MB-435 cells harboring aberrant Stat3 and treated with S3I-M2001, compared to minimal effect on normal NIH3T3, human breast epithelial MCF-10A, breast cancer MDA-MB-453, and human umbilical vein endothelial cells (HUVEC) that do not contain aberrant Stat3. Validating that the S3I-M2001-induced apoptosis is due to interaction with its

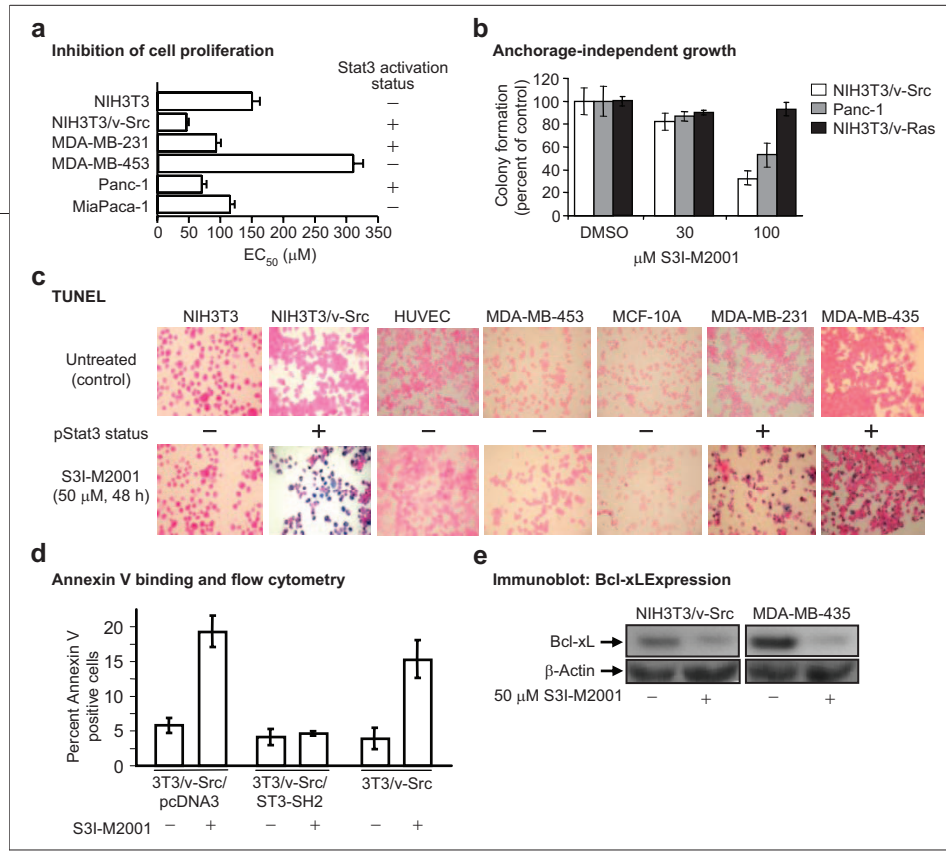

Figure 7. Effect of S3I-M2001 on cell viability, malignant transformation, apoptosis, and Bcl-xL expression: a) IC_{50} values for the S3I-M2001-induced loss of cell viability determined by WST-1 assay; b) anchorage-independent growth in soft-agar suspension of malignant cells (NIH3T3/v-Src, Panc-1, and NIH3T3/v-Ras) treated with or without S3I-M2001 every 3 days; c) TUNEL staining for DNA damage in normal NIH3T3 and NIH3T3/v-Src, human endothelial (HUVEC), breast cancer cells (MDA-MB-453, MDA-MB-231, and MDA-MB-435), and the normal breast epithelial MCF-10A cells treated with or without S3I-M2001 for 48 h, Stat3 activity status is indicated as (+), pStat3 (activated), (−), no Stat3 activity; d) annexin V binding and flow cytometry of NIH3T3/v-Src fibroblasts transfected with empty vector, pcDNA3 (3T3/v-Src/pcDNA3) or the Stat3 SH2 domain (3T3/v-Src/ST3-SH2) for 4 h or untransfected (3T3/v-Src) and treated with or without 100 μM S3I-M2001 for additional 24 h; e) SDS-PAGE and Western blot analysis for Bcl-xL in NIH3T3/v-Src and MDA-MB-435 cells. Images shown are representative of two to three independent studies. Values are the mean and standard deviation of three to four replicate experiments.

molecular target (Stat3 SH2 domain), NIH3T3/v-Src fibroblasts (3T3/v-Src) transiently transfected with a plasmid encoding the Stat3 SH2 domain (3T3/v-Src/ST3-SH2) and treated with S3I-M2001 showed diminished apoptosis (Figure 7, panel d, compare middle two bars) compared to mock-transfected (3T3/v-Src/pcDNA3) (Figure 7, panel d, left two bars) or untransfected cells (Figure 7, panel d, right two bars). Moreover, Western blot analysis showed diminished Bcl-xL expression, a known Stat3-regulated and antiapoptotic gene (*32*), in the S3I-M2001-treated NIH3T3/v-Src and MDA-MB-435 cells (Figure 7, panel e; *in situ* immunohistochemical staining in Supplementary Figure S4), suggesting repressed Bcl-xL expression is part of the underlying mechanism for the S3I-M2001-induced apoptosis.

Given Stat3's importance in tumor growth and tumor progression (*33*), matrigel assay using Bio-Coat migration chambers showed significant S3I-M2001-induced inhibition of the migration of NIH3T3/v-Src (76%), MDA-MB-231 (37%), and Panc-1 (21%) and the invasion of NIH3T3/v-Src (28%), MDA-MB-231 (48%), and Panc-1 (38%) cells harboring constitutively active (Figure 8, panel a; percent inhibition in parentheses defined in "Methods" section). Furthermore, in xenograft models of human breast (MDA-MB-231 cells that harbor aberrant Stat3) tumor-bearing mice, the *i.v.* injection of S3I-M2001 at 5, 10, and 20 mg kg^{-1}, but not vehicle (control) every 2 or 3 days for 26 days, strongly inhibited growth of tumors (Figure 8, panel b). Animals remained viable at the highest (20 mg kg^{-1}) dose applied. DNA-binding assay with EMSA analysis and SDS/AGE-Western blotting of lysates from residual tumor tissues extracted from representative control and treated mice showed abrogated Stat3 activity and pTyr levels in S3I-M2001-treated tumors (T1 and T2) (Figure 8, panels c and d). These findings together demonstrate S3I-M2001 induces antitumor cell effects and tumor regression in part by targeting the Stat3 SH2 domain and inhibiting Stat3-mediated tumor processes (*3, 6, 7, 17, 22, 34, 35*). Moreover, S3I-M2001 compares favorably with other Stat3 SH2 domain-targeting small-molecule inhibitors, including S3I-201, which was obtained by computational modeling and virtual chemical library screening (*13*), and represents a significant improvement over its peptidomimetic predecessors (*10*).

We provide the first study of the cellular processing and stability of aberrant Stat3 in malignant cells within the context of inhibition by a chemical probe that has implications for the many human tumor cells, including the human breast and pancreatic cancer cells that harbor aberrant Stat3. The general applicability of the current study to other previously identified

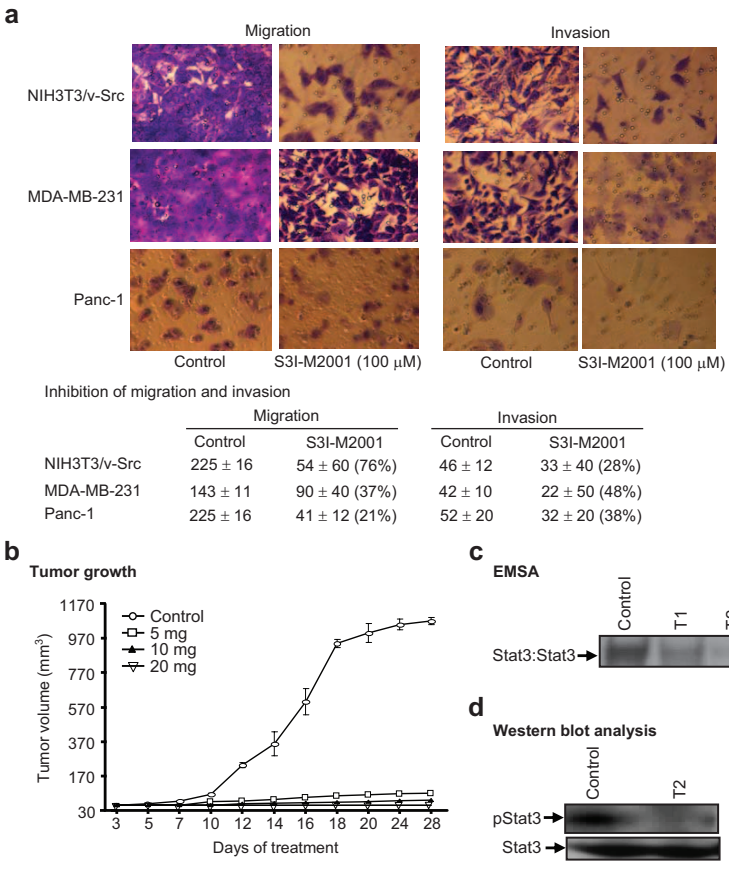

Inhibition of migration and invasion

	Migration		Invasion	
	Control	S3I-M2001	Control	S3I-M2001
NIH3T3/v-Src	225 ± 16	54 ± 60 (76%)	46 ± 12	33 ± 40 (28%)
MDA-MB-231	143 ± 11	90 ± 40 (37%)	42 ± 10	22 ± 50 (48%)
Panc-1	225 ± 16	41 ± 12 (21%)	52 ± 20	32 ± 20 (38%)

Figure 8. S3I-M2001 suppresses malignant cell migration and invasion and inhibits growth of human breast tumor xenografts: a) Viral Src-transformed mouse fibroblasts (NIH3T3/v-Src), human breast cancer (MDA-MB-231), and pancreatic cancer (Panc-1) cells were seeded for studies in migration on filters or invasion on matrigel-coated filters in Bio-Coat chambers and treated with or without S3I-M2001 (100 mM) for 24. Cells on the other side of filters were photographed (upper panel) and quantified under light microscope (lower panel; percent inhibition in parentheses); human breast (MDA-MB-231) tumor bearing mice were given S3I-M2001 (5, 10, and 20 mg kg^{-1}) *i.v.* every 2 or 3 days. b) Tumor sizes, measured every 2 or 3 days, were converted to tumor volumes and plotted against treatment days. c) EMSA analysis of Stat3 DNA-binding activity in lysates from tumor tissues extracted from one control and two residual treated tumors (T1 and T2) 3 days after the last S3I-M2001 (5 mg kg^{-1}) injection. d) SDS-PAGE/Western blot analysis of whole-cell lysates from control or residual treated (T2) tumor tissue and probing for pTyr705Stat3 and Stat3. Values are the mean and standard deviation of three independent experiments each in duplicates or replicates of 12 tumor-bearing mice in each group. Data are representative of two to three independent experiments. Bands of Stat3:DNA complexes, pStat3, and Stat3 are shown.

Stat3 inhibitors, including the g-quartet oligonucleotides (*36*), peptide aptamers (*37*), platinum (IV) complexes (*11, 12*), and STA-21 (NSC 628869) (*38*), however, is unclear, as those other agents have different modes of inhibition of Stat3 from S3I-M2001. Altogether, our studies establish the proof-of-concept for the antitumor effects of S3I-M2001 that correlate with disruption of constitutively active Stat3:Stat3 dimers, while using S3I-M2001 as a chemical probe to investigate the molecule dynamics of termination of Stat3 function following inhibition.

METHODS

Cells and Reagents. Normal mouse fibroblasts (NIH3T3) and counterparts transformed by v-Src transformed (NIH3T3/v-Src), v-Ras (NIH3T3/v-Ras), or overexpressing the human EGFR (NIH3T3/hEGFR), human breast cancer (MDA-MB-435, MDA-MB-453, MDA-MB-231 and MDA-MB-468), immortalized human

breast epithelial cells, MCF-10A, and pancreatic cancer (Panc-1) cell lines have all been previously described (*9–12, 17, 18, 39*). Human umbilical vein cells (HUVEC) were a kind gift Dr. S. Chellappan of Moffitt Cancer Center and Research Institute (Tampa, FL). Cells were grown in Dulbecco's modified Eagle's medium (DMEM) containing 5% iron-supplemented bovine calf serum; MCF-10A cells were grown in DMEM:F12 media supplemented with 5% FBS, 10 $\mu g\ mL^{-1}$ insulin, 500 $ng\ mL^{-1}$ hydrocortisone, 20 $ng\ mL^{-1}$ EGF, and 100 $ng\ mL^{-1}$ cholera toxin. HUVEC cells were grown in Ham's F12k medium with 2 mM L-glutamine containing 1.5 $g\ L^{-1}$ sodium bicarbonate and supplemented with 0.1 $mg\ mL^{-1}$ heparin and 0.03 $mg\ mL^{-1}$ endothelial cell growth supplement, and 10% FBS. WST-1 viability assay reagent was obtained from Roche, and the TUNEL assay kit was from BD Biosciences Pharmingen. Each treatment condition is a single dose at the indicated concentration or 0.1% DMSO (vehicle) as control. Anti-Hook2 antibody was from Santa Cruz.

Plasmids. The pLucTKS3 and pLucSRE luciferase reporters have been previously reported (*17, 19*).

Compound Synthesis. The design strategy for the construction of the oxazole scaffold was carried out using standard synthetic procedures, following the principle of rapid incorporation of structural diversity into an acyclic precursor, with subsequent late stage aromatization providing the desired heteroaryl array (*40*).

Recombinant Baculoviruses, Infection of Sf-9 Insect Cells and Cytosolic Lysate Preparation. Infection of Sf-9 cells with Stat1, Stat3, Jak1, and c-Src recombinant baculoviruses and preparation of the cell lysates containing activated Stat1 or Stat3 have been previously described (*9, 41*).

Nuclear Extract Preparation and Gel Shift Assays. Nuclear extract preparation from cells and EMSA were carried out as previously described (*9–12, 16, 18, 39*) (additional information in Supporting Information). Bands corresponding to DNA-binding activities were scanned and quantified for each concentration of compound and plotted as percent of control (vehicle) against concentration of compound, from which the IC_{50} values were derived, as previously reported (*9, 10, 39*).

Immunoprecipitation (i.p.) and SDS-PAGE/Western Blot Analysis. Whole-cell lysates prepared in boiling SDS sample-loading buffer, i.p. from lysates using monoclonal anti-Stat3 antibody (Cell Signaling Technology), and the probing of nitrocellulose membranes with primary antibodies and detection of horseradish peroxidase-conjugated secondary antibodies by enhanced chemiluminescence (Amersham Biosciences) were done, as previously described (*13, 17, 19, 41*). The probes used were anti-Stat3 (Santa Cruz), anti-pTyr705Stat3 (Cell Signaling Technology), anti-YFP (Santa Cruz), anti-Bcl-xL, anti-pSrc, anti-Src, anti-pJak1, anti-Jak1, anti-pEr1/2 and anti-Erk1/2, and β-Actin (Cell Signaling Technology) antibodies.

Dissociation–Reassociation Analysis. The dissociation–reassociation analysis with EMSA analysis was performed, as previously done (*10, 20*).

Lck-SH2 Domain ELISA Assay. An ELISA assay for the binding of Lck-SH2 domain with its conjugate phosphopeptide, biotinyl-ϵ-Ac-EPQpYEEIEL-OH, was carried out, as previously described (*13, 21*). Absorbance reading (450 nm) for the peroxidase reaction was determined with an ELISA plate reader.

Fluorescence Microscopy. NIH3T3/vSrc cells either were stably transfected with Stat3-YFP construct (*24*) or, growing in 96-well plates on chamber slides, were transiently transfected with the Stat3-YFP plasmid (*24*) using Lipofectamine 2000 for 24 h according to the manufacturer's protocol (Roche), treated with or without S3I-M2001 for different times, and examined under Nikon Eclipse TE200 fluorescence microscope (Nikon). Images were captured and processed by NIKON NIS element-Basic research software.

Confocal Microscopy. NIH3T3/hEGFR cells were grown in multicell plates and treated with or without S3I-M2001 for 3 h prior to stimulation by rhEGF (10 $ng\ mL^{-1}$) for 10 min or NIH3T3/vSrc cells were grown in multicell plates or chamber slides. Cells were fixed with 4% paraformaldehyde for 15 min and processed for confocal microscopy (details are presented in Supporting Information).

Soft-Agar Colony Formation Assay. Colony formation assays were carried out in six-well dishes, and colonies were enumerated as previously described (*19*). Treatment with S3I-M2001 was initiated 1 day after seeding cells in soft-agar suspension by adding 75–100 μL of medium with or without compound and repeated every 3 days, until large colonies were evident.

Cell Viability Assay, TUNEL Analysis, and Annexin V Binding and Flow Cytometry. WST-1 assay for viability (Roche), and terminal nucleotidyl transferase-mediated dUTP nick end labeling (TUNEL) staining (Roche) and Annexin V binding with flow cytometry for apoptosis (BD Biosciences) were performed according to the manufacturer's protocol (further details in Supporting Information).

Cell Migration and Matrigel Invasion Assays. Cell migration and invasion experiments were carried out using Bio-Coat migration chambers (Becton Dickinson) of 24-well companion plates with cell culture inserts containing 8 μm pore size filters, according to the manufacturer's protocol. Details are provided in Supporting Information. Percent inhibition is calculated as $100 - y$, where y equals residual number of stained cells in the treated/total number in the control $\times 100$.

Mice and *in Vivo* Tumor Studies. Six-week-old female athymic nude mice were purchased from Harlan and maintained in the institutional animal facilities approved by the American Association for Accreditation of Laboratory Animal Care. Athymic nude mice were injected subcutaneously in the left flank area with 5×10^6 human breast cancer MDA-MB-231 cells in 100 μL of PBS. After 5–10 days, tumors of a diameter of 3 mm were established. Animals were grouped so that the mean tumor sizes in all groups were nearly identical, given S3I-M2001 *i.v.* at 5, 10, and 20 mg/kg every 2 or every 3 days for 26 days and monitored every 2 or 3 days, and tumor sizes were measured with calipers. Tumor volume was calculated according to the formula $V = 0.52a^2b$, where a is the smallest superficial diameter and b is the largest superficial diameter.

Acknowledgment: We thank all colleagues and members of our laboratory for the stimulating discussions and the University of Central Florida Burnett School of Biomedical Sciences Transgenic Animal Facility for assistance with the animal work. This work was supported by the National Cancer Institute Grant CA106439 (J.T.).

Supporting Information Available: This material is available free of charge *via* the Internet.

REFERENCES

1. Darnell, J. E., Jr. (1996) The JAK-STAT pathway: summary of initial studies and recent advances, *Recent Prog. Horm. Res. 51*, 391–403.
2. Darnell, J. E., Jr. (1997) STATs and gene regulation, *Science 277*, 1630–1635.
3. Darnell, J. E. (2005) Validating Stat3 in cancer therapy, *Nat. Med. 11*, 595–596.
4. Bowman, T., Garcia, R., Turkson, J., and Jove, R. (2000) STATs in oncogenesis, *Oncogene 19*, 2474–2488.
5. Buettner, R., Mora, L. B., and Jove, R. (2002) Activated STAT signaling in human tumors provides novel molecular targets for therapeutic intervention, *Clin. Cancer Res. 8*, 945–954.

6. Yu, H., and Jove, R. (2004) The STATS of Cancer-New molecular targets come of age, *Nat. Rev. Cancer 4*, 97–105.
7. Turkson, J. (2004) STAT proteins as novel targets for cancer drug discovery, *Expert Opin. Ther. Targets 8*, 409–422.
8. Haura, E. B., Turkson, J., and Jove, R. (2005) Mechanisms of disease: Insights into the emerging role of signal transducers and activators of transcription in cancer, *Nat. Clin. Pract. Oncol. 2*, 315–324.
9. Turkson, J., Ryan, D., Kim, J. S., Zhang, Y., Chen, Z., Haura, E., Laudano, A., Sebti, S., Hamilton, A. D., and Jove, R. (2001) Phosphotyrosyl peptides block Stat3-mediated DNA-binding activity, gene regulation and cell transformation, *J. Biol. Chem. 276*, 45443–45455.
10. Turkson, J., Kim, J. S., Zhang, S., Yuan, J., Huang, M., Glenn, M., Haura, E., Sebti, S., Hamilton, A. D., and Jove, R. (2004) Novel peptidomimetic inhibitors of signal transducer and activator of transcription 3 dimerization and biological activity, *Mol. Cancer Ther. 3*, 261–269.
11. Turkson, J., Zhang, S., Palmer, J., Kay, H., Stanko, J., Mora, L. B., Sebti, S., Yu, H., and Jove, R. (2004) Inhibition of constitutive signal transducer and activator of transcription 3 activation by novel platinum complexes with potent anti-tumor activity, *Mol. Cancer Ther. 3*, 1533–1542.
12. Turkson, J., Zhang, S., Mora, L. B., Burns, A., Sebti, S., and Jove, R. (2005) A novel platinum compound inhibits constitutive Stat3 signaling and induces cell cycle arrest and apoptosis of malignant cells, *J. Biol. Chem. 280*, 32979–32988.
13. Siddiquee, K., Zhang, S., Guida, W. C., Blaskovich, M. A., Greedy, B., Lawrence, H. R., Yip, M. L., Jove, R., McLaughlin, M. M., Lawrence, N. J., Sebti, S. M., and Turkson, J. (2007) Selective chemical probe inhibitor of Stat3, identified through structure-based virtual screening, induces antitumor activity, *Proc. Natl. Acad. Sci. U.S.A. 104*, 7391–7396.
14. Becker, S., Groner, B., and Muller, C. W. (1998) Three-dimensional structure of the Stat3beta homodimer bound to DNA, *Nature 394*, 145–151.
15. Jones, G., Willett, P., Glen, R. C., Leach, A. R., and Taylor, R. (1997) Development and validation of a genetic algorithm for flexible docking, *J. Mol. Biol. 267*, 727–748.
16. Yu, C. L., Meyer, D. J., Campbell, G. S., Larner, A. C., Carter-Su, C., Schwartz, J., and Jove, R. (1995) Enhanced DNA-binding activity of a Stat3-related protein in cells transformed by the Src oncoprotein, *Science 269*, 81–83.
17. Turkson, J., Bowman, T., Garcia, R., Caldenhoven, E., De Groot, R. P., and Jove, R. (1998) Stat3 activation by Src induces specific gene regulation and is required for cell transformation, *Mol. Cell. Biol. 18*, 2545–2552.
18. Garcia, R., Bowman, T. L., Niu, G., Yu, H., Minton, S., Muro-Cacho, C. A., Cox, C. E., Falcone, R., Fairclough, R., Parson, S., Laudano, A., Gazit, A., Levitzki, A., Kraker, A., and Jove, R. (2001) Constitutive activation of Stat3 by the Src and JAK tyrosine kinases participates in growth regulation of human breast carcinoma cells, *Oncogene 20*, 2499–2513.
19. Turkson, J., Bowman, T., Adnane, J., Zhang, Y., Djeu, J. Y., Sekharam, M., Frank, D. A., Holzman, L. B., Wu, J., Sebti, S., and Jove, R. (1999) Requirement for Ras/Rac1-Mediated p38 and c-Jun N-Terminal Kinase Signaling in Stat3 Transcriptional Activity Induced by the Src Oncoprotein, *Mol. Cell. Biol. 19*, 7519–7528.
20. Shuai, K., Horvath, C. M., Huang, L. H., Qureshi, S. A., Cowburn, D., and Darnell, J. E., Jr (1994) Interferon activation of the transcription factor Stat91 involves dimerization through SH2-phosphotyrosyl peptide interactions, *Cell 76*, 821–828.
21. Lee, T. R., and Lawrence, D. S. (2000) SH2-directed ligands of the Lck tyrosine kinase, *J. Med. Chem. 43*, 1173–1179.
22. Bromberg, J. F., Horvath, C. M., Besser, D., Lathem, W. W., and Darnell, J. E., Jr (1998) Stat3 activation is required for cellular transformation by v-src, *Mol. Cell. Biol. 18*, 2553–2558.
23. Nam, S., Buettner, R., Turkson, J., Kim, D., Cheng, J. Q., Muehlbeyer, S., Hippe, F., Vatter, S., Merz, K. H., Eisenbrand, G., and Jove, R. (2005) Indirubin derivatives inhibit Stat3 signaling and induce apoptosis in human cancer cells, *Proc. Natl. Acad. Sci. U.S.A. 102*, 5998–6003.
24. Herrmann, A., Sommer, U., Pranada, A. L., Giese, B., Kuster, A., Haan, S., Becker, W., Heinrich, P. C., and Muller-Newen, G. (2004) STAT3 is enriched in nuclear bodies, *J. Cell Sci. 117*, 339–349.
25. Gelman, M. S., Kannegaard, E. S., and Kopito, R. R. (2002) A principal role for the proteasome in endoplasmic reticulum-associated degradation of misfolded intracellular cystic fibrosis transmembrane conductance regulator, *J. Biol. Chem. 277*, 11709–11714.
26. Bence, N. F., Sampat, R. M., and Kopito, R. R. (2001) Impairment of the ubiquitin-proteasome system by protein aggregation, *Science 29*, 1552–1555.
27. Bennett, E. J., Bence, N. F., Jayakumar, R., and Kopito, R. R. (2005) Global impairment of the ubiquitin-proteasome system by nuclear or cytoplasmic protein aggregates precedes inclusion body formation, *Mol. Cell 17*, 351–365.
28. Szebenyi, G., Wigley, W. C., Hall, B., Didier, A., Yu, M., Thomas, P., and Kramer, H. (2007) Hook2 contributes to aggresome formation, *BMC Cell Biol. 8*, 19.
29. Johnston, J. A., Ward, C. L., and Kopito, R. R. (1998)Aggresomes: a cellular response to misfolded proteins, *J. Cell. Biol. 143*, 1883–1898.
30. Garcia-Mata, R., Bebok, Z., Sorscher, E. J., and Sztul, E. S. (1999) Characterization and dynamics of aggresome formation by a cytosolic GFP-chimera, *J. Cell. Biol. 146*, 1239–1254.
31. Ciechanover, A., Orian, A., and Schwartz, A. L. (2000) Ubiquitin-mediated proteolysis: biological regulation via destruction, *Bioessays 22*, 442–451.
32. Catlett-Falcone, R., Landowski, T. H., Oshiro, M. M., Turkson, J., Levitzki, A., Savino, R., Ciliberto, G., Moscinski, L., Fernandez-Luna, J. L., Nuñez, G., Dalton, W. S., and Jove, R. (1999) Constitutive activation of Stat3 signaling confers resistance to apoptosis in human U266 myeloma cells, *Immunity 10*, 105–115.
33. Huang, C., Cao, J., Huang, K. J., Zhang, F., Jiang, T., Zhu, L., and Qiu, Z. J. (2006) Inhibition of STAT3 activity with AG490 decreases the invasion of human pancreatic cancer cells in vitro, *Cancer Sci. 97*, 1417–1423.
34. Turkson, J., and Jove, R. (2000) STAT proteins: novel molecular targets for cancer drug discovery, *Oncogene 19*, 6613–6626.
35. Scholz, A., Heinze, S., Detjen, K. M., Peters, M., Welzel, M., Hauff, P., Schirner, M., Wiedenmann, B., and Rosewicz, S. (2003) Activated signal transducer and activator of transcription 3 (STAT3) supports the malignant phenotype of human pancreatic cancer, *Gastroenterology 125*, 891–905.
36. Jing, N., Li, Y., Xu, X., Sha, W., Li, P., Feng, L., and Tweardy, D. J. (2003) Targeting Stat3 with G-quartet oligodeoxynucleotides in human cancer cells, *DNA Cell Biol. 22*, 685–696.
37. Nagel-Wolfrum, K., Buerger, C., Wittig, I., Butz, K., Hoppe-Seyler, F., and Groner, B. (2004) The interaction of specific peptide aptamers with the DNA binding domain and the dimerization domain of the transcription factor Stat3 inhibits transactivation and induces apoptosis in tumor cells, *Mol. Cancer Res, 2*, 170–182.
38. Song, H., Wang, R., Wang, S., and Lin, J. (2005) A low-molecular-weight compound discovered through virtual database screening inhibits Stat3 function in breast cancer cells, *Proc. Natl. Acad. Sci. U.S.A. 102*, 4700–4705.
39. Garcia, R., Yu, C. L., Hudnall, A., Catlett, R., Nelson, K. L., Smithgall, T., Fujita, D. J., Ethier, S. P., and Jove, R. (1997) Constitutive activation of Stat3 in fibroblasts transformed by diverse oncoproteins and in breast carcinoma cells, *Cell Growth Differ. 8*, 1267–1276.
40. Wipf, P., and Miller, C. P. (1993) Stereospecific synthesis of peptide analogs with allo-threonine and D-allo-threonine residues, *J. Org. Chem. 58*, 3604–3606.

41. Zhang, Y., Turkson, J., Carter-Su, C., Smithgall, T., Levitzki, A., Kraker, A., Krolewski, J. J., Medveczky, P., and Jove, R. (2000) Activation of Stat3 in v-Src Transformed Fibroblasts Requires Cooperation of Jak1 Kinase Activity, *J. Biol. Chem. 275*, 24935–24944.